Robotica (2015) volume 33, pp. 578–598. © Cambridge University Press 2014
doi:10.1017/S0263574714000472

Compensating the flexibility uncertainties of a cable suspended robot using SMC approach

M. H. Korayem*, M. Taherifar and H. Tourajizadeh

Robotic Research Laboratory, Center of Excellence in Experimental Solid Mechanics and Dynamics, School of Mechanical Engineering, Iran University of Science and Technology, Tehran, Iran

(Accepted February 6, 2014. First published online: March 5, 2014)

SUMMARY

A sliding mode controller is designed to compensate for the flexibility uncertainties of a cable robot and improve its tracking performance. Of the most significant sources of these uncertainties are the elasticity of the cables and the flexibility of the joints. A favorable approach to improve the accuracy of the system is first to model the cable and joint flexibilities and then convert the model uncertainties into parametric uncertainties. Parametric uncertainties are the product of imprecise flexibility coefficients and are finally neutralized by a sliding mode controller. The flexibility in cables is modeled by considering the longitudinal vibration of the time-varying length cables. A simulation study is carried out to confirm the presented model and the positive effect of the designed controller. Then the impact of these uncertainties on the dynamic load carrying capacity (DLCC) of the robot is examined and compared for different cases. Finally, experimental tests are conducted on the IUST (Iran University of Science and Technology) cable-suspended robot to validate the presented theories and simulation results.

KEYWORDS: Cable suspended robot; Sliding Mode Control (SMC); Uncertainty; Elastic cables; Flexible joints.

1. Introduction

Cable-suspended parallel robots (CPRs), in which the links are replaced by a series of cables, were initially studied by Albus in 1993.[1] The issue of controlling and developing these types of robots has recently been a matter of controversial debate. Cable robots have high stiffness, great load capability, and acceptable accuracy. However, the parallel structure and the utilization of cables bring some complexities and nonlinearities into robot dynamic model. These complexities along with some model and parametric uncertainties increase the probability of tracking error. So in this paper, first, a study of the dynamic model of a 6-DOF (degree of freedom) cable-suspended robot is presented and then, two of these main uncertainties, i.e., flexibility in joints and flexibility in cables are modeled. Improvements in modeling increase the precision of robot dynamic model so that the probability of the model uncertainties is reduced. Next, the sliding mode controller is designed and performance and robustness of the controller are examined.

Robot control is a key competence for robot manufacturers and a lot of development is done to increase robot performance and reduce robot cost.[2] However, some constraints such as the incapability of cables to withstand compressive load and the emergence of uncertainties and flexibilities introduce more complexity in controlling the system and underscore the necessity of an accurate controller for better tracking. Feedback linearization method, sliding mode, and adaptive control are three of the most common and applicable robot control methods for the extreme nonlinear dynamic of the robot. Yanai focused on feedback control method for under-constrained cable robots.[3] In another research, a feedback linearization controller is designed for a cable-suspended robot with 6 DOFs with positive input constraints.[4] Feedback linearization method exhibits an appropriate and quick performance in controlling nonlinear systems such as cable robots; however, it is not a robust method against system

* Corresponding author. E-mail: hkorayem@iust.ac.ir

https://doi.org/10.1017/S0263574714000472 Published online by Cambridge University Press

uncertainties. Zarebidoki used the adaptive control approach for controlling a cable-suspended robot by considering the uncertainty in the exact value of mass and inertia of the end-effector.[5] Although the employed adaptive controller is efficient enough to overcome system parameter uncertainties, it is not a robust controller to compensate for the unstructured and modeling uncertainties. Many authors employed the sliding mode control (SMC) known as robust method against parametric and model uncertainties and external disturbances. Pi and Wang tried to precisely control the motion of a hydraulic parallel robot with 6 DOFs. They used sliding mode method with regards to the existence of error in the modeling of hydraulic actuators and uncertain payload.[6] By studying a three-cable robot acted in three-dimensional (3D) space, Gorman presented the kinematic and dynamic modeling of this cable array robot. Then he used the model to design a sliding mode controller.[7] To control dual-stage planar cable robot with 6 DOFs (presented by The National Institute of Standards and Technology (NIST)), the sliding mode method is employed as a robust controller in the presence of unknown disturbances (such as sea wave motion).[8] Agrawal also modeled the dynamics and proposed a design control method of a helicopter which carries a cable-suspended robot. He demonstrated that, by using a sliding mode controller, the cable robot can be stabilized, even when the helicopter has an undefined and non-uniform motion.[9] A sliding mode controller is designed for a cable-suspended robot with 6 DOFs as a balancing controller against the given system uncertainties.[10,11]

An examination of the use of SMC on robots indicated that this method not only compensates for the effects of uncertainties and disturbances of the system, but also it helps the system perform a precise trajectory tracking. Uncertainties in the robot parameters such as mass, geometry, or inertia, and uncertainty in the model are big challenges in trajectory tracking. Parametric uncertainties have limited effects on robot performance. However, there are some model uncertainties in the robot that have great impact on control accuracy. Inaccurate and incomplete dynamic model, which is an outcome of ignoring the flexibility of the modeling, increases the probability of model uncertainty. So far, a certain body of research has focused on the modeling of flexibility and reducing model uncertainties. Yeon modeled and controlled the flexible joints in a serial robot with 6 DOFs.[12] Korayem investigated controlling of a cable robot with flexible joints by means of the feedback linearization method. However, since the used feedback linearization method was not robust, the required modification to improve the performance of the robot has not been introduced.[13] Other researchers have also presented a model for elastic cables. Zi proposed dynamic modeling and active control of a CPR with six flexible cables.[14] Zhang *et al.* presented the model of a cable transporter system with arbitrarily varying cables' length and applied Lyapunov controller to dissipate the vibratory energy.[15,16] They proposed a complete model; however, it was only tested on a cable transporter system with 3 DOFs. The flexibility in the cables of a cable-suspended robot is modeled and the result of small motion of the end-effector is discussed by the aid of delta flatness theory.[17,18] However, it is not a proper method to investigate the cable flexibility, since they linearized the system dynamics around the path and this assumption will work for only small movements. Du *et al.* proposed a dynamic model for cable-driven parallel manipulators with cables of slowly time-varying length.[19,20] They used finite difference approximation to convert the final partial differential equations (PDEs) characterizing the dynamics of a cable into ordinary differential equations (ODEs) that was not an exact and accurate method. Also they assumed that cable length is changed slowly and smoothly, which was a limiting assumption.

As seen above, the existing literature has ignored something. In this paper, flexible joints and flexible cables of a 6-cable flexible cable-suspended robot with 6 DOFs are modeled. In flexible joint case, elastic joints are modeled as rotational springs with unspecified spring coefficients (as parametric uncertainty). The flexibility of the cables is taken into account by modeling the cable's longitudinal vibrations. The challenging problem of solving the vibrating equation of the cables with time-varying length is solved by considering the large motion and small vibrating deformation simultaneously. The proposed method applicable in any cable velocity (not just slow and smooth one) improves the accuracy and speed of the calculation process for the first time implemented on a cable-suspended robot. The non-homogeneous PDEs that characterize the dynamics of a cable are converted to ODEs by the aid of Fourier transforms (analytical solution). The uncertainties rising from flexibility of the cable robot are then compensated using sliding mode controller as a proper controlling strategy for nonlinear dynamic system with uncertainties. By the aid of a series of simulation studies, destructive impact of the mentioned uncertainties on the dynamic performance of the robot is investigated. The positive effect of the proposed controller in neutralizing the flexibility uncertainties is demonstrated

https://doi.org/10.1017/S0263574714000472 Published online by Cambridge University Press

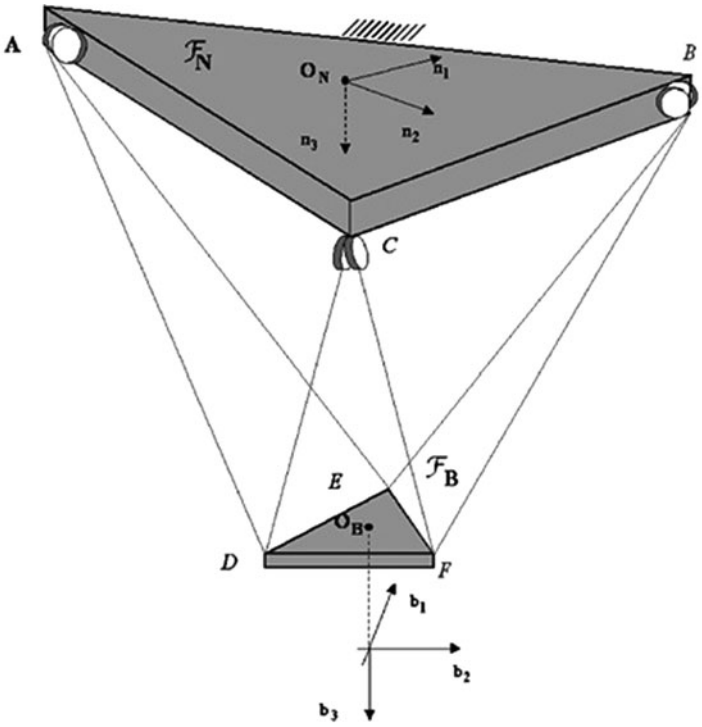


Fig. 1. Schematic of a 6-cable robot.[13]

by comparing the dynamic load carrying capacity (DLCC) of the robot in each case. Finally, the validity and efficiency of the proposed algorithm are verified by conducting some experimental tests in Iran University of Science and Technology Cable Robot (ICaSbot).

In Section 2, in addition to dynamic study of the cable robot in its rigid form, the dynamic modeling of the robot with elastic joints and elastic cables is presented. Section 3 presents the simulation results of the trajectory tracking, a comparison of the DLCCs of the robot in different cases, and a comparison of simulation and experimental results.

2. Formulation

The dynamic model and controller are improved step by step from the rigid robot to the flexible one.

2.1. Dynamic modeling

2.1.1. Dynamics of rigid robot The examined spatial cable robot has a triangular shaped end-effector, as shown in Fig. 1, which is suspended through six cables and has 6 DOFs. The direction and position of the end-effector relative to the reference coordinate are stated by six variables of $X = [x, y, z, \psi, \theta, \varphi]^T$. Three transitional movements along the Cartesian coordinate and three rotational movements around the general coordinate are supported by end-effector.

A Newton–Euler equation brings the system the following dynamic equation:[21]

$$D(X)\ddot{X} + C\left(X, \dot{X}\right)\dot{X} + g(X) = -S_J^T(X)\,T, \tag{1}$$

where $D(X)$ is the inertia matrix of the system, $C(X, \dot{X})\dot{X}$ is the vector of Coriolis and centripetal terms, $g(X)$ is the vector of gravity terms, and T is the vector of cables tension.[21]

$$D(X) = \begin{bmatrix} mI_3 & 0 \\ 0 & P^T I P \end{bmatrix}; C(X, \dot{X})\dot{X} = \begin{bmatrix} 0_{3\times 1} \\ P^T\{I\dot{P}\dot{o} + (P\dot{o}) \times I(Po)\} \end{bmatrix}; g(X) = \begin{bmatrix} 0 \\ 0 \\ -mg \\ 0_{3\times 1} \end{bmatrix};$$

https://doi.org/10.1017/S0263574714000472 Published online by Cambridge University Press

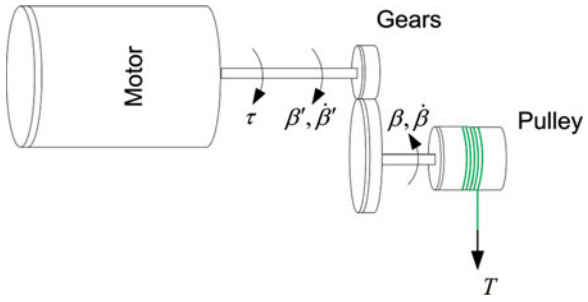


Fig. 2. Schematic of the motor with gearbox.

$$S_J = \left[\frac{\partial L_i}{\partial x_j}\right]_{i\times j}; P = \begin{bmatrix} 1 & 0 & -\sin\theta \\ 0 & \cos\psi & \sin\psi\cos\Theta \\ 0 & -\sin\psi & \cos\psi\cos\Theta \end{bmatrix}; \dot{o} = \begin{bmatrix} \dot{\Psi} \\ \dot{\Theta} \\ \dot{\varphi} \end{bmatrix}, \tag{2}$$

where S_J is the Jacobean of the inverse kinematic model, X is the vector of DOFs of the system, m is the mass of the end-effector, I is the moment of inertia of the end-effector and L is the length of the cables. The relation between the angle of the pulleys, β, and the position of the end-effector can be written as:

$$\begin{aligned} \dot{\beta} &= \frac{\partial \beta}{\partial X}\dot{X}, \\ \ddot{\beta} &= \mathrm{d}/\mathrm{d}t(\partial\beta/\partial X)\dot{X} + (\partial\beta/\partial X)\ddot{X}. \end{aligned} \tag{3}$$

The dynamics of the motor is[13]

$$T = \frac{1}{r}\left[\tau - J\left(\frac{\mathrm{d}}{\mathrm{d}t}\left(\frac{\partial\beta}{\partial X}\right)\dot{X} + \frac{\partial\beta}{\partial X}\ddot{X}\right) - C_f\frac{\partial\beta}{\partial X}\dot{X}\right], \tag{4}$$

where J is the diagonal matrix of rotary inertia of the motors, C_f is the viscous friction coefficient of the motors, and τ is the vector of motor torque. By substituting Eq. (4) in Eq. (1),

$$D(X)\ddot{X} + C(X,\dot{X})\dot{X} + g(X) = -S_J^T(X)\frac{1}{r}\left[\tau - J\left(\frac{\mathrm{d}}{\mathrm{d}t}\left(\frac{\partial\beta}{\partial X}\right)\dot{X} + \frac{\partial\beta}{\partial X}\ddot{X}\right) - C_f\frac{\partial\beta}{\partial X}\dot{X}\right]. \tag{5}$$

2.1.2. Flexible joint dynamics There is always a degree of clearance or elasticity between the actuators and pulleys. This elasticity is often caused by the gearbox used to convert the rotational speed and applied torque ratio (Fig. 2). There is a reduction gear installed on each motor in the manufactured robot. So, by using the Newton–Euler equation and considering the gearbox ratio as N, it can be written as:

$$J'\ddot{\beta}' = \tau - T_e - C_f\dot{\beta}', \tag{6}$$

$$J\ddot{\beta} = NT_e - T.r, \tag{7}$$

where J, β are the rotary inertia and angle of the pulleys, respectively, J', β' are the same variables for motor, N is the gearbox ratio, r is the radius of the pulleys, C_f is the damping or friction coefficient, T is the tension applied to the cables, T_e is the transmitted torque and τ is the torque produced by the motors.

Since there is no elasticity in this modeling,

$$\dot{\beta}' = N\dot{\beta}. \tag{8}$$

https://doi.org/10.1017/S0263574714000472 Published online by Cambridge University Press

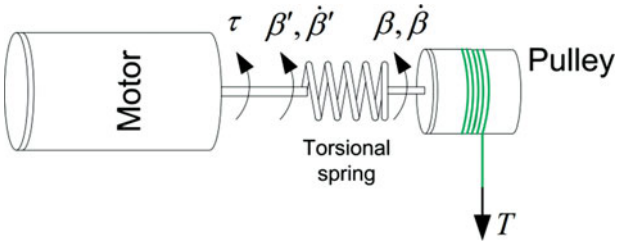


Fig. 3. Schematic of elastic joint for cable robot.

So

$$(J + N^2 J')\ddot{\beta} + C_f N^2 \dot{\beta} = N\tau - T \times r. \tag{9}$$

As mentioned above the gearbox between the motor and pulley introduces flexibility in the model. The reduction gear is used to increase the torque of the motors and the dynamic of motors is considered to be linear here. But the gearbox brings flexibility into the joints which makes the dynamic of the system more nonlinear. By considering a rotational spring between the motor and pulley, this flexibility in the joints can be modeled as below (Fig. 3).[13]

Using Newton–Euler approach it can be written as:[13]

$$J\ddot{\beta} + k(\beta - \beta') = -rT, \tag{10}$$

$$J'\ddot{\beta}' - k(\beta - \beta') = \tau - C_f \dot{\beta}'. \tag{11}$$

Equation (10) specifies the dynamic of the pulleys and Eq. (11) shows motor dynamic, where J, β are the rotary inertia and angle of the pulleys, respectively, J', β' are the same variables for motor, k is the elasticity coefficient of the spring between the motor and the pulley, r is the radius of the pulleys, C_f is the viscous damping coefficient, T is the tension applied to the cables, and τ is the torque produced by the motors. Combining Eqs. (10) and (11),

$$J\ddot{\beta} + J'\ddot{\beta}' = \tau - rT - C_f \dot{\beta}'. \tag{12}$$

Based on Eq. (3),[13]

$$T = \frac{1}{r}\left(\tau - J'\ddot{\beta}' - C_f\dot{\beta}' - J\left(\frac{\mathrm{d}}{\mathrm{d}t}\left(\frac{\partial\beta}{\partial X}\right)\dot{X}\right) + \frac{\partial\beta}{\partial X}\ddot{X}\right). \tag{13}$$

Equation (13) determines the required amount of tension that should be applied to the cables to achieve the desired position of the end-effector.

2.1.3. Flexible cable dynamic As mentioned above, some researchers have modeled the elasticity of the cables considering time-varying cable lengths in their modeling. Since the cables are always in tension mode, the impact of longitudinal vibrations on end-effector movements is considerably higher than transverse vibration. Also, the transverse vibration often occurs in cranes where there are swings and wind effects. With this in mind, in this paper, the flexibility of the cables of a cable robot is modeled by considering longitudinal vibrations of the cables with variable lengths. Modeling is done by using Newton method and considering the simultaneous deformations of large motion of the end-effector together with deformation related to the cable vibration. The resultant PDEs are then solved by the aid of analytic solution of Fourier transform with an acceptable process speed.

First, assumptions for modeling cable vibration in cable robot. Changes of the cable length due to longitudinal vibration are much less than large deflections of the cables; the cables are homogeneous, i.e., the cable parameters such as mass per length and elasticity module can be considered uniform along the cable length. The velocity of each element of the cable is assumed to be the transport speed of the end-effector plus time derivative of the longitudinal vibration.

https://doi.org/10.1017/S0263574714000472 Published online by Cambridge University Press

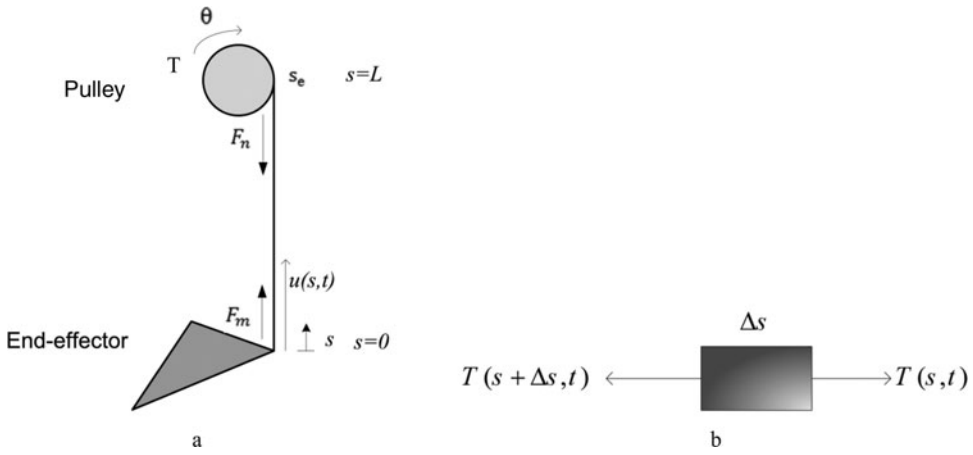


Fig. 4. (a) Scheme of elastic cable; (b) force balance of a small element in the cable.

Free body diagram of small element of elastic cable is used to derive the elastic cable model (Fig. 4(b)). By using Newton's law it can be expressed as[16]

$$T(s+\Delta s,t)-T(s,t)=\rho\Delta s(-\ddot{s}_e+\ddot{u}), \tag{14}$$

where s is the coordinate of cable elongation, T is the vector of cables' tension, ρ is mass per unit length of the cable, s_e is the vector of the coordinates of the contact point of cable and pulley, and u is displacement due to the longitudinal vibration of the cable. Applying Taylor series and ignoring higher order terms, we get

$$T(s+\Delta s,t)=T(s,t)+\frac{\partial T(s,t)}{\partial s}\Delta s, \tag{15}$$

so that,

$$\frac{\partial T(s,t)}{\partial s}\Delta s=\rho\Delta s(-\ddot{s}_e+\ddot{u})\Rightarrow\frac{\partial T(s,t)}{\partial s}=\rho(-\ddot{s}_e+\ddot{u}). \tag{16}$$

Using strain–stress relationship, it can be stated that,[16]

$$T(s,t)=EA\frac{\partial u(s,t)}{\partial s}, \tag{17}$$

where E is Young's modulus of the cable (elasticity modulus) and A is the cross-section area of the cable. By substituting Eq. (17) in Eq. (16), the governing PDE of the cable vibration can be extracted as

$$EA\frac{\partial^2 u(s,t)}{\partial s^2}=\rho(-\ddot{s}_e+\ddot{u}). \tag{18}$$

As it can be seen, the relationship between longitudinal vibration and large deflection of a flexible cable robot appears as a non-homogenous PDE and it is attributed to the instantaneous change of length of cables. On the other hand, s_e is the length of the cable in each time step so it is substituted by L in equations.

$$EA\frac{\partial^2 u(s,t)}{\partial s^2}-\rho\frac{\partial^2 u(s,t)}{\partial t^2}=-\rho\ddot{L}. \tag{19}$$

https://doi.org/10.1017/S0263574714000472 Published online by Cambridge University Press

The boundary conditions can be found based on Fig. 4(a). The vibration near the pulley is always zero; so $u(L, t) = 0$, also the forces near the pulley (F_n) and end-effector (F_m) can be defined as:[17]

$$\begin{aligned} EA\frac{\partial u(s,t)}{\partial s}\Big|_{s=0} &= F_m, \\ EA\frac{\partial u(s,t)}{\partial s}\Big|_{s=L} &= F_n. \end{aligned} \tag{20}$$

Obtaining the tension of the cable, near the pulley (F_n), is the main goal of inverse dynamic of flexible cable robot. After calculating the cable tension near the end-effecter (F_m) from the given path, the mentioned non-homogeneous PDE (Eq. (19)) should be solved considering the following boundary conditions:

$$u(L, t) = 0, \quad EA\frac{\partial u(s,t)}{\partial s}\Big|_{s=0} = F_m. \tag{21}$$

It is impossible to find a closed-form analytical solution for the governing PDE. So, first the PDE is converted to ODE by the aid of Fourier transform. Then, using numerical methods and getting an approximate solution of ODE, the inverse Fourier transform is used to get the final solution. The used Fourier transform for converting the obtained PDE of Eqs. (19) and (21) is given in Appendix A. Fourier transform of Eq. (19) with the boundary conditions of Eq. (21) gives

$$\frac{\mathrm{d}^2U(n,t)}{\mathrm{d}t^2} + \frac{EA}{\rho}\lambda_n^2 U(n,t) = \sqrt{\frac{2}{L}}\frac{F_m}{\rho} + \frac{\ddot{L}}{\lambda_n}(-1)^n, \tag{22}$$

where n is the number of considered vibrating modes of the cables and λ_n is

$$\lambda_n = \frac{(2n-1)\pi}{2L}. \tag{23}$$

The following initial conditions are used to solve the ODE in Eq. (22):

$$U(n, 0) = 0, \dot{U}(n, 0) = 0. \tag{24}$$

After calculating *U (n, t)*, the inverse Fourier transform (Appendix A) is used to obtain the final solution:

$$u(s,t) = \sqrt{\frac{1}{2L}}U(0,t) + \sqrt{\frac{2}{L}}\sum_{n=1}^{\infty} U(n,t)\cos\lambda_n s. \tag{25}$$

Also, tension near the pulley (F_n) can be obtained by considering Eq. (20):

$$F_n = -EA\sqrt{\frac{2}{L}}\sum_{n=1}^{\infty}\lambda_n U(n,t)(-1)^{n+1} \tag{26}$$

In the direct dynamics of flexible cable, the mentioned PDE in Eq. (19) with its boundary conditions (Eq. (27)) should be solved:

$$EA\frac{\partial u(s,t)}{\partial s}\Big|_{s=0} = F_m, \; EA\frac{\partial u(s,t)}{\partial s}\Big|_{s=L} = F_n. \tag{27}$$

Here the cables tension near the pulley (F_n) is obtained by Eq. (26) and the desired amount of cables tension near the end-effector (F_m) is used as its boundary conditions. The Fourier cosine transform is applied to solve the PDE, and converting it to ODE form (Appendix B),

$$\rho\frac{\mathrm{d}^2U(n,t)}{\mathrm{d}t^2} + EA\lambda_n^2 U(n,t) = -\frac{2}{L}\left[F_m + (-1)^{n+1}F_n\right] = 0, \tag{28}$$

https://doi.org/10.1017/S0263574714000472 Published online by Cambridge University Press

where λ_n and its initial condition are defined as

$$\lambda_n = \frac{n\pi}{L}; \tag{29}$$

$$U(n,0) = 0, \dot{U}(n,0) = 0. \tag{30}$$

After solving the ODE of Eq. (28) with initial conditions in Eq. (30), inverse Fourier cosine transform is used (Appendix B):

$$u(s,t) = \frac{U(0,t)}{2} + \sum_{n=1}^{\infty} U(n,t)\cos\frac{n\pi}{L}s. \tag{31}$$

2.2. Control scheme

The flexibility uncertainty of the cable-suspended robot is compensated using a nonlinear robust control strategy, i.e., sliding mode. There are several advantages in SMC: high-speed response, good transient performance, insensitivity to certain parameter variations, and external disturbances. This control method is a robust and an efficient control strategy for nonlinear dynamic of the cable robot in presence of parametric uncertainties of cable elasticity. The sliding surface (s_s) and Lyapunov function are defined as below:[10]

$$s_s = \left(\frac{\mathrm{d}}{\mathrm{d}t} + \lambda\right)^{n-1} \tilde{X}, \tag{32}$$

where

$$\tilde{X} = X - X_d. \tag{33}$$

The problem of tracking $X \equiv X_d$ is equivalent to that of remaining on the surface s_s for all $t > 0$. Indeed $s_s \equiv 0$ represents a linear differential equation whose unique solution is $\tilde{X} \equiv 0$.

Since the dynamic equation of cable robot is of second order, so $n = 2$.

$$s_s = (\dot{X} - \dot{X}_d) + \lambda(X - X_d), \tag{34}$$

where s_s is a 6×1 vector and λ is a 6×6 diagonal matrix of control gain.

Now the Lyapunov function (V) is defined as

$$V = \frac{1}{2} s_s^T s_s. \tag{35}$$

So,

$$\dot{V} = s_s^T \dot{s}_s \;\Rightarrow\; \dot{V} = s_s^T[\ddot{X} - \ddot{X}_d + \lambda(\dot{X} - \dot{X}_d)]. \tag{36}$$

Here by considering the dynamic of rigid system and by replacing $\ddot{X}$ from Eq. (1) into Eq. (36),

$$\dot{V} = s_s^T\left[D^{-1}(X)(-S_J^T(X)\,T - C(X,\dot{X}) - g(X)) - \ddot{X}_d + \lambda(\dot{X} - \dot{X}_d)\right]. \tag{37}$$

To guarantee Lyapunov stability of the robot, the control torques must be designed to meet the following condition:

$$\dot{V} < 0 \quad \text{for } s_s \neq 0. \tag{38}$$

To meet this goal and making $\dot{V}$ negative, the following control law should be adopted:

$$T = -(S_J^T)^{-1}[D(X)\{\ddot{X}_d - \lambda(\dot{X} - \dot{X}_d) - K.\mathrm{sgn}(s)\} + C(X,\dot{X})\dot{X} + g(X)]. \tag{39}$$

https://doi.org/10.1017/S0263574714000472 Published online by Cambridge University Press

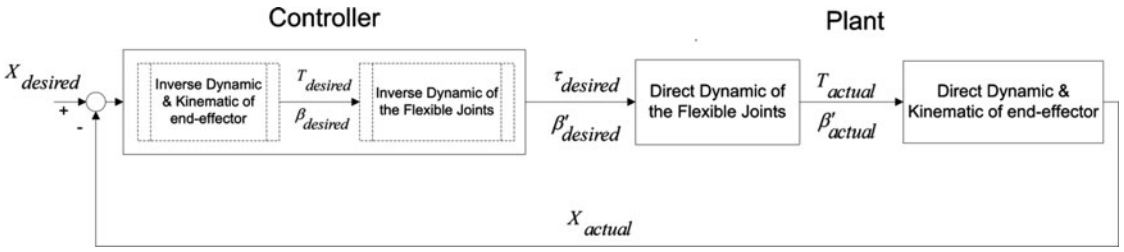


Fig. 5. Control block-diagram of cable suspended robot with flexible joints.

Since the number of actuators is equivalent to the number of DOFs, the Jacobean matrix (S_J) is square and invertible. K is a 6×6 diagonal matrix of control gain. It can be easily shown that this control law makes $\dot{V}$ negative.[10]

2.2.1. Flexible joint control It can easily be shown that a flexible robot is stable and it is possible to control the system with a feedback of the main DOFs of the system, i.e., position and orientation of the end-effector $X = [x, y, z, \psi, \theta, \varphi]^T$ since there is no internal dynamics in the system.[22] So, by considering the main DOFs of the robot, the rigid robot control is improved for the flexible dynamic. The same approach is used to define the sliding surface in flexible joint model as Eq. (34) and V, $\dot{V}$ are defined as Eqs. (35) and (36). On the other hand, it is shown that in flexible joint dynamic, the relationship between DOFs and motor torque is defined by

$$D(X)\ddot{X} + C(X, \dot{X})\dot{X} + g(X) = -S_J^T(X)\frac{1}{r}\left[\tau - J'\ddot{\beta}' - J\ddot{\beta} - C_f\dot{\beta}'\right]. \tag{40}$$

So,

$$\dot{V} = s_s^T\left[D^{-1}(X)\left\{-S_J^T(X)\frac{1}{r}\left[\tau - J'\ddot{\beta}' - J\ddot{\beta} - C_f\dot{\beta}'\right] - C(X, \dot{X}) - g(X)\right\} - \ddot{X}_d + \lambda(\dot{X} - \dot{X}_d)\right]. \tag{41}$$

And to make $\dot{V}$ negative, the following control law should be adopted:

$$\begin{aligned}\tau = {} & -r \times (S_J^T)^{-1}[D(X)\{\ddot{X}_d - \lambda(\dot{X} - \dot{X}_d) - K.\mathrm{sgn}(s)\} + C(X, \dot{X})\dot{X} + g(X)] \\ & + J'\ddot{\beta}' + J\ddot{\beta} + C_f\dot{\beta}',\end{aligned} \tag{42}$$

where K is the control gain.

The control block diagram of a flexible-joints robot can be seen in Fig. 5. Control signal (τ) and desired motor rotation are calculated in control section. In direct dynamic of flexible joint, the actual cable tension and actual motor rotation are calculated. Finally, the actual path of the end-effector is calculated using the direct dynamics and kinematics equations.

2.2.2. Flexible cable control As in the flexible joints control, the sliding surface and the Lyapunov function V and its derivation $\dot{V}$ should be defined first as Eqs. (34)–(36). On the other hand, the cable tension near the end-effector (F_m) is calculated by considering the end-effector dynamic:

$$D(X)\ddot{X} + C(X, \dot{X})\dot{X} + g(X) = -S_J^T(X)F_m. \tag{43}$$

So,

$$\dot{V} = s_s^T[D^{-1}(X)(-S_J^T(X)F_m - C(X, \dot{X}) - g(X)) - \ddot{X}_d + \lambda(\dot{X} - \dot{X}_d)]. \tag{44}$$

To make $\dot{V}$ negative, the following control law should be adopted:

$$F_m = -(S_J^T)^{-1}[D(X)\{\ddot{X}_d - \lambda(\dot{X} - \dot{X}_d) - K.\mathrm{sgn}(s)\} + C(X, \dot{X})\dot{X} + g(X)]. \tag{45}$$

https://doi.org/10.1017/S0263574714000472 Published online by Cambridge University Press

Table I. Circular path equation.

$t < 4$	$t \geq 4$	$z = 0.45$
$x = 0.05\cos(4\pi t^2/64)$	$x = 0.05\cos(4\pi(-t+8)^2/64)$	$\psi = 0$
$y = 0.05\sin(4\pi t^2/64)$	$y = -0.05\sin(4\pi(-t+8)^2/64)$	$\Theta = 0$
		$\varphi = 0$

Table II. Cable robot's parameter.

Name	Symbol	Value	Unit
Moment of inertia of the triangle end-effector	I	$I_{xx} = I_{yy} = 0.0018$ $I_{zz} = 0.0036$	kgm^2
Radius of the motor	r	diag[0.0015]	m
Damping coefficient	C_f	diag[0.01]	Nm/rad
Rotary inertia of the motor	J	diag[0.0008]	kgm^2
Mass of the end-effector	m	1.09	kg
Control gain	λ	[10,10,10,10,10,10]	Per second
Control gain	K	[50,50,50,50,50,50]	m/s^2

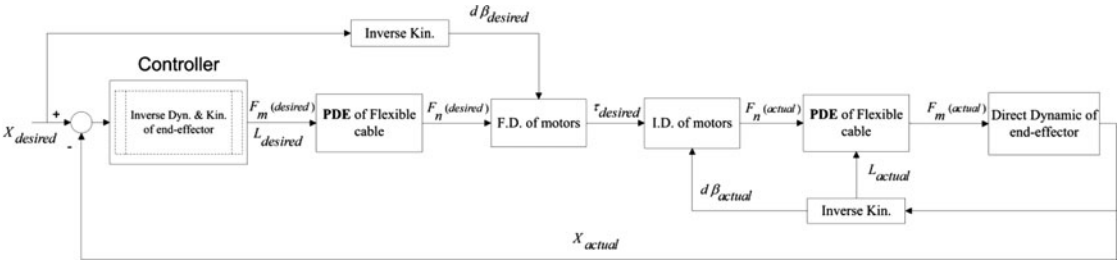


Fig. 6. Control block-diagram of cable robot with elastic cables.

The control block diagram of a flexible cable robot is presented in Fig. 6. After calculating the desired path and by using the inverse dynamics and kinematics equations, cable tension near the end-effector (F_m) and the desired cable length (L_{desired}) can be calculated. It should be noted that in elastic cable, the tensions are not the same at both sides of the cable as a result of flexibility.[17] Therefore, by solving the PDE of vibration of cable and satisfying the desired conditions, the desired cable tension near the pulley (F_n) is obtained. After solving the motor dynamic and getting the desired torque, again, the motor dynamics with actual input is solved and so the actual cable tension near the pulley (F_n) is calculated. Now, by solving the vibration PDE (direct dynamic of flexible cable) with a new boundary condition, the actual cable tension near the end-effector can be estimated and by the aid of direct dynamics of the end-effector, the actual path can be estimated.

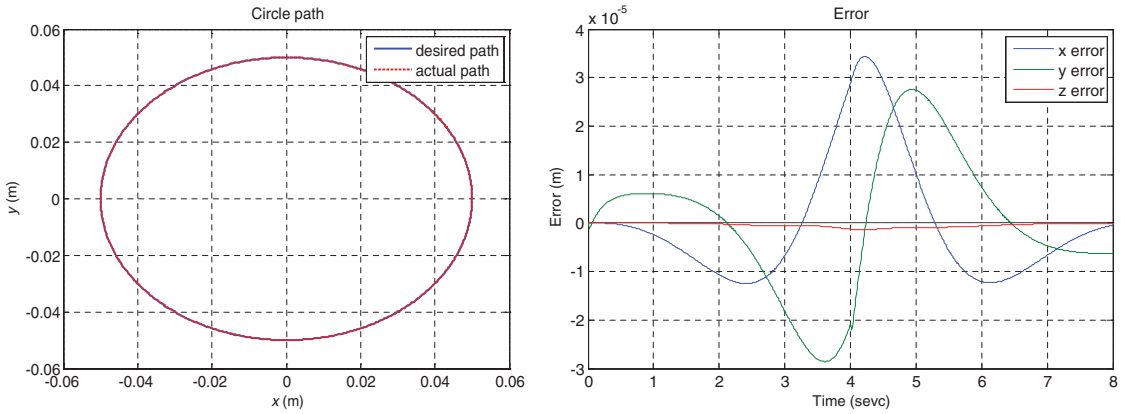
3. Simulation Experimental Results

3.1. Sliding mode control simulation

To investigate the controller performance in tracking, a circular path is taken as a desired trajectory. The path equation provided in SI unit is shown in Table I. The robot specifications are given in Table II. Moment of inertia of the end-effector (I) is a diagonal matrix because of the triangle shape of the end-effector. They were calculated by experimental tests around its local axes. Damping coefficient (c), coefficient of joint elasticity (k), and elasticity modulus of the cables (E) are obtained by parameter identification through modeling of the flexibility in the MATLAB and comparing the output of the experiment with the simulation as a result of a unique input.

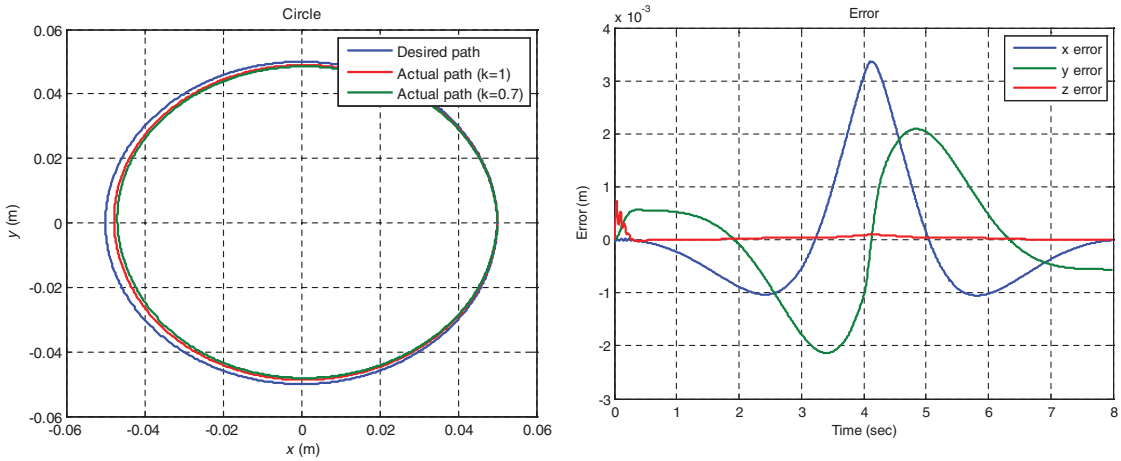
It can be seen from the trajectory tracking and error profile in Fig. 7 that the sliding mode controller has an accurate and proper performance in the absence of any uncertainty. Also the motor torque is shown in Fig. 9(a).

https://doi.org/10.1017/S0263574714000472 Published online by Cambridge University Press



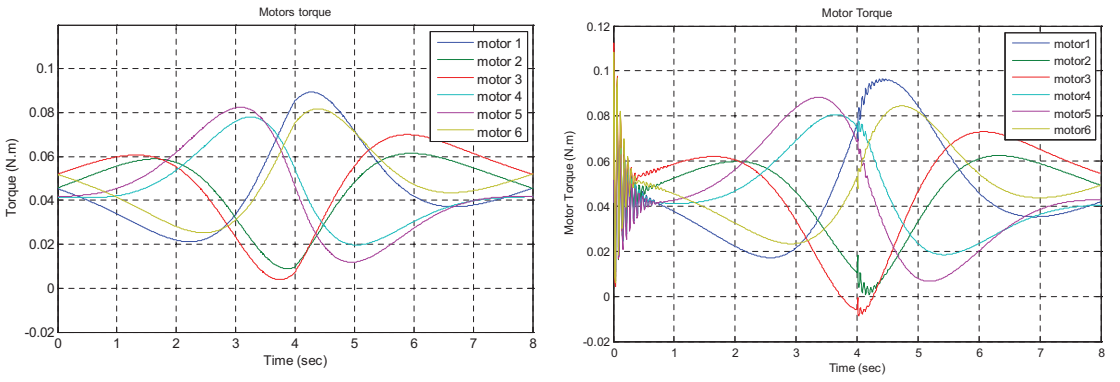
(a) (b)

Fig. 7. (a) The comparison of the trajectory for a predefined circular path; (b) the related errors.



(a) (b)

Fig. 8. (a) The trajectory tracking for a circular path in flexible joints simulation tracking errors for $k = 1$.



(a) (b)

Fig. 9. The comparison between the rigid and flexible joints' motor's torque: (a) rigid case; (b) flexible joint case.

https://doi.org/10.1017/S0263574714000472 Published online by Cambridge University Press

Table III. Flexible joint cable robot's parameter.

Name	Symbol	Value	Unit
Rotary inertia of the motor & pulley	J, J'	diag[0.0008]	kg m^2
Coefficient of joint elasticity	k	diag[0.7] $< k <$ diag[1]	N m/rad
Control gain	λ	[25,25,25,25,25,25]	Per second
Control gain	K	[70,70,70,70,70,70]	m/s^2

Table IV. Cable robot and elastic cable parameters.

Name	Symbol	Value	Unit
Elasticity modulus of the cables	E	$1.65 \times 10^7 - 1.65 \times 10^8$	N/m^2
Cable density	ρ	0.0125	kg/m
Cable diameter	d	3	mm
Number of considered longitudinal mode shapes	n	2	
Control gain	λ	[2.5,7.5,35,5,0.5,5]	Per second
Control gain	K	[12.5,10,100,25,10,5]	m/s^2

3.2. Flexible joint simulation

Here the tracking performance of the cable robot with flexible joints is simulated for a circular movement of the end-effector (Table I). The impact of the joint elasticity uncertainty on tracking error and motor torque is investigated. It should be noted that a specified range for k (coefficient of joint elasticity) or E (elasticity modulus of cables) as the main parametric uncertainties is required.

On the other hand, it is impossible to determine the exact value of spring coefficient by experimental tests. So, the range of k is obtained by trial and error and parameter identification; in $k = 1.3$ the results were roughly rigid, and in $k = 0.5$, the highest acceptable deviation was observed. Therefore, the range of [0.7, 1] is considered as the range of joint flexibility uncertainty (Table III).

The input–output path and tracking error are shown in Fig. 8. It can be seen that by reducing the k coefficient and increasing the flexibility, the tracking error rises and deviates from the rigid response. As it is shown in tracking error, the joint flexibility has little impact on z error.

As it can be seen from motor torque graphs in both rigid and flexible tracking (Fig. 9), there are some oscillations in motor torque during the 0–0.5 s. These oscillations occur because of the flexibility effect of the joints. However, they are damped since there is a damper in modeling of the joints. The robot should apply greater torque in flexible joint tracking.

3.3. Flexible cable simulation

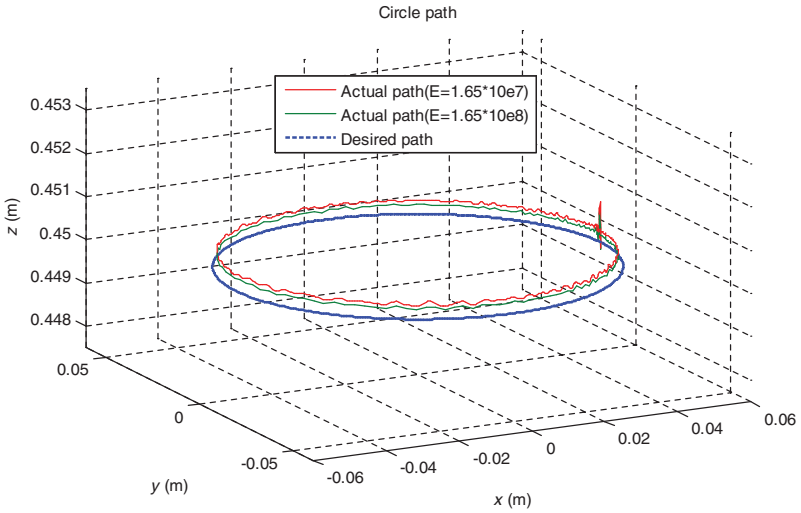
To simulate the tracking performance of the cable robot with elastic cables, the circular path in Table I is assumed. Cable parameters and control gains are shown in Table IV. Elasticity modulus of the cables and cable density were estimated by some experimental tests on real robot cable. So, the range $[1.65 \times 10^7, 1.65 \times 10^8]$ is used to simulate the uncertainty of the cable elasticity.

As it can be seen in Fig. 10, cable vibration introduces significant oscillation in all dimensions. However, there is an offset with respect to the desired path in z direction that is due to the longitudinal vibrations.

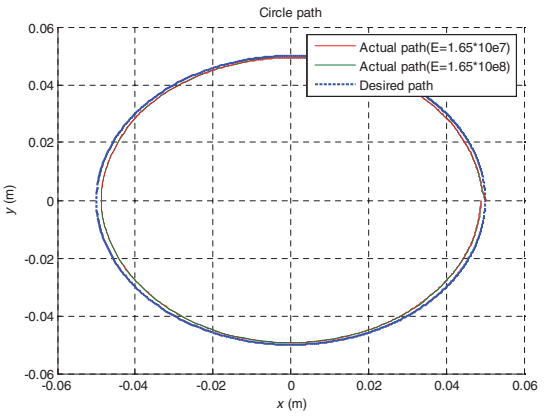
Figures 11(a) and 11(b) give a comparison of the first motor torque to the rigid case and tensions in both sides of the first cable.

As seen, while the mean value of the first motor torque in the flexible case is roughly equal to that of the rigid case, it oscillates about this mean value due to the vibration of cables. These oscillations continue to the end of the end-effector movement because of an absence of structural damping. Cable longitudinal vibrations also bring oscillations into the cable tension. As expected, and clearly seen in Fig. 11(b), tensions on both end-sides of the cables are unequal, and the amount of tension near the pulley is high. It is also seen that the magnitude of cable tension force near the end-effector has started from zero, which is related to the method used. The observations also indicate that by reducing the elasticity modulus which increases the flexibility of the cables, the result moves away from the

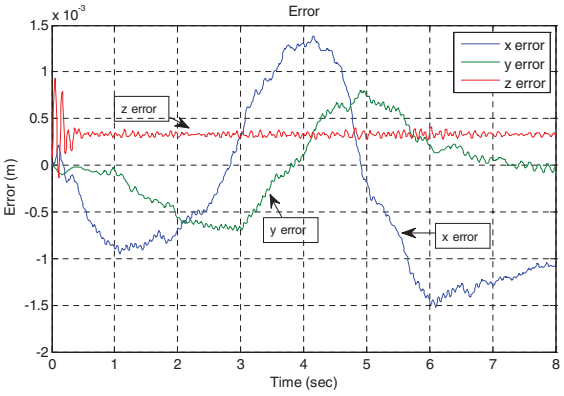
https://doi.org/10.1017/S0263574714000472 Published online by Cambridge University Press



(a)

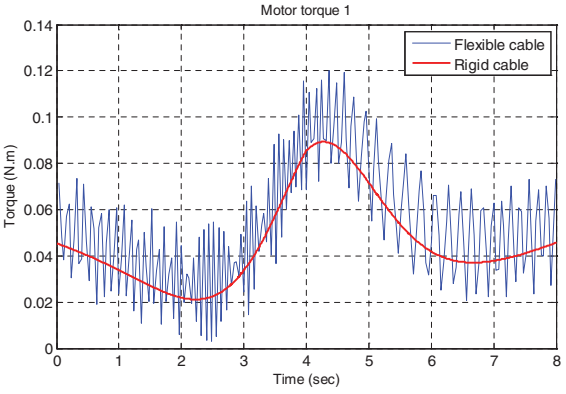


(b)

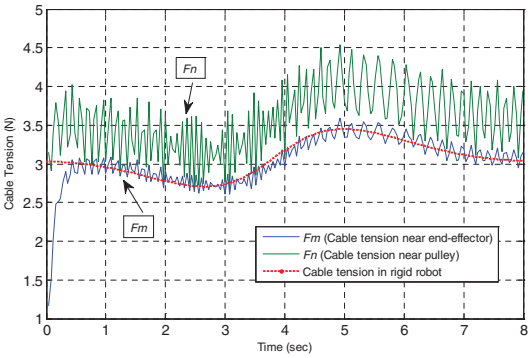


(c)

Fig. 10. (a), (b) Trajectory tracking for a circular path in flexible cable simulation; (c) tracking errors for $E = 165 \times 10\,\text{e}7$.



(a)



(b)

Fig. 11. (a) The torque of first motor in both rigid and flexible cable tracking tensions of the end-sides of the first cable compared to rigid case.

https://doi.org/10.1017/S0263574714000472 Published online by Cambridge University Press

Table V. Motor specification.

Name	Symbol	Value	Unit
Maximum allowable error bound of tracking	R	0.01	m
Free running angular velocity of the motors	ω_n	286	rad/ sec
Stall torque of the motors	τ_s	10	Nm

rigid-state response, and the amplitude of vibrations also rises. Thus, the oscillations in the tension of the cables and torque of the motors rise as well.

3.4. DLCC calculation

Maximum DLCC of the robot is one of the most important parameters in robotic science and industry that represents the robot capability for carrying the heaviest load with specified accuracy. This parameter that illustrates the applicability of the robot, is used to evaluate the robot power and accuracy simultaneously. It is expected that the robot carries the highest possible load on the predefined path. So it is required to employ the highest power of the motors while the required accuracy is satisfied simultaneously. In this paper, by calculating the DLCC for both rigid and flexible robots, the effects of flexibility uncertainties are investigated. Also, the DLCC of the robot with sliding mode controller and the robot with the feedback linearization controller in refs. [23] and [24] are compared. This comparison illustrates the effect of robust controller to compensate for the flexibility uncertainties. DLCC is defined based on two dynamic constraints, including motor torque constraint and accuracy constraint. The actuator torque constraint is formulated based on typical torque-speed characteristics of a direct current (DC) motor.[13]

$$\tau_u = k_1 - k_2\dot{q}, \tag{46}$$

where τ_u is the upper bound of actuator constraint. The coefficient k_i is defined as[13]

$$k_1 = T_s; \;\; k_2 = \frac{T_s}{w_{nl}}, \tag{47}$$

where T_s is the stall torque and w_{nl} is the free running angular speed of the motor. Also, by defining the appropriate bound of error, the accuracy constraint is addressed as well. The following flowchart can be employed to determine the DLCC of a cable robot.

As shown in Fig. 12, the desired path is defined and then the control signal (τ) is calculated through sliding mode method. Next, the upper bound of the actuator constraint and the tracking error are calculated. Both accuracy and actuator constraints should be saturated simultaneously by choosing the proper control gains. The predefined load should be increased gradually in the loop with an iterative strategy. This increase lasts until one of the torque or accuracy constraints is violated. The final load is the robot DLCC.[23]

3.4.1. Simulation of DLCC. Following the algorithm above, the calculation of DLCC according to the torque upper limits (torque constraint) and accuracy constraint is done for rigid and flexible robot. The specifications of cable robot motors are shown in Table V and the circle path of Table I is taken as the desired path.

For the rigid case, the motor torque and accuracy of tracking are saturated for the load equal to DLCC = 4.65 kg.

As shown in Table VI, the DLCC of a flexible joint cable robot with higher spring coefficient is estimated at about 4.15 kg. As seen in Fig. 13, the first motor is saturated at the middle of the simulation and the tracking error becomes saturated slightly after the start of tracking. Maximum DLCC of the flexible joint cable robot with lower spring coefficient is about 3.18 kg, considerably lower than that of the rigid case. So, it can be concluded that by decreasing the spring coefficient, which consequently increases the robot flexibility, the capability of the robot to carry the load (DLCC) dwindles.

https://doi.org/10.1017/S0263574714000472 Published online by Cambridge University Press

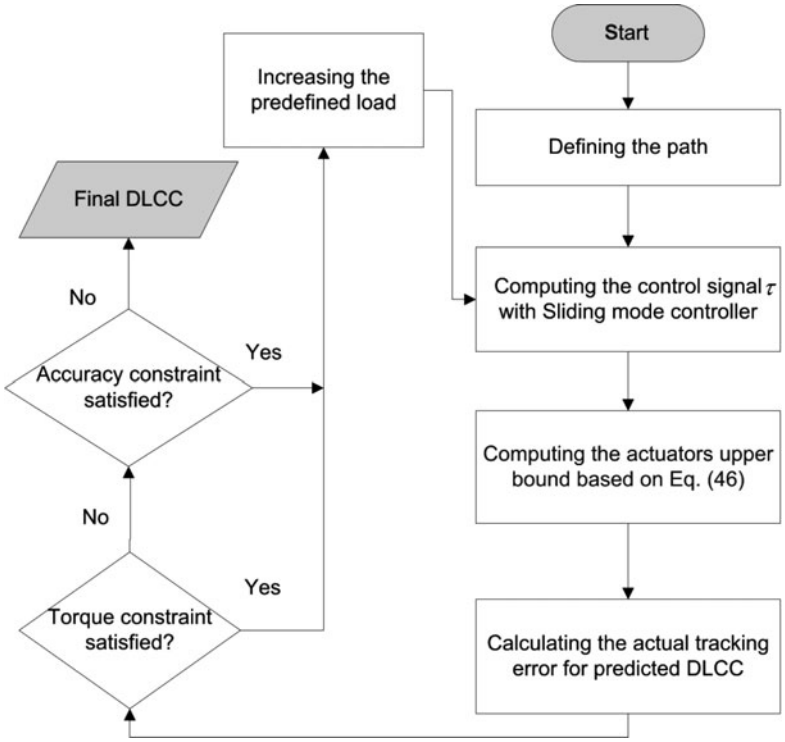


Fig. 12. DLCC algorithm.

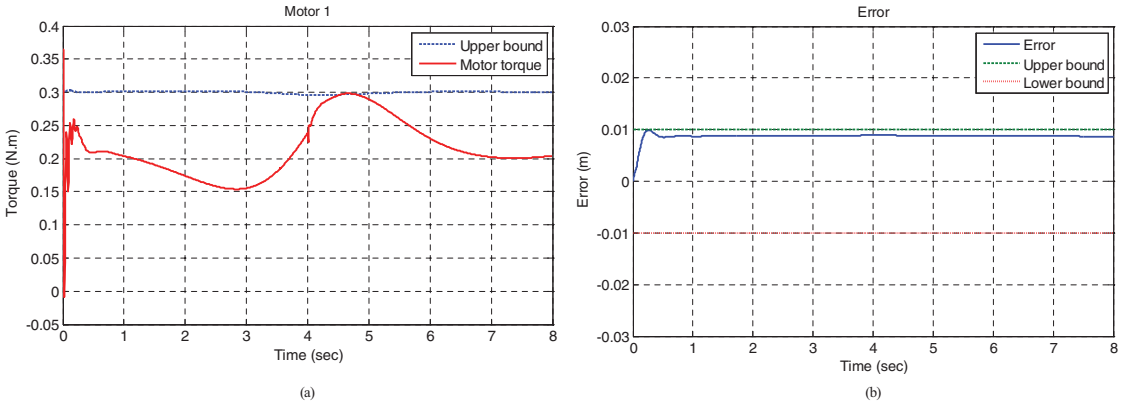


Fig. 13. Saturation profiles of flexible joint simulation for $k = 1$; (a) torque constraint; (b) accuracy constraint.

Table VI. DLCC and simulation parameters for flexible joint cases.

Name	Coefficient of joint elasticity (k)	Control gain (λ)	Control gain (K)	DLCC (kg)
Case 1	1 [N m/rad]	[23,23,23,23,23,23]	[182,182,182,10,10,10]	**4.15**
Case 2	0.6 [N m/rad]	[23,23,23,23,23,23]	[182,182,182,10,10,10]	**3.28**

For the flexible cable robot, the maximum DLCC is compared for two different samples with different moduli of elasticity (Table VII). This comparison investigates the effect of cable flexibility on the DLCC of the robot, which is equipped with SMC controller.

In the first case with high modulus of elasticity, the first saturation occurs for the first motor (Fig. 14) for the load equal to DLCC = 3.85. The difference between this amount and rigid robot DLCC of about 0.8 kg illustrates the bad impact of cable flexibility on robot performance. The maximum DLCC of the flexible cable robot with lower elasticity modulus (higher flexibility) is about

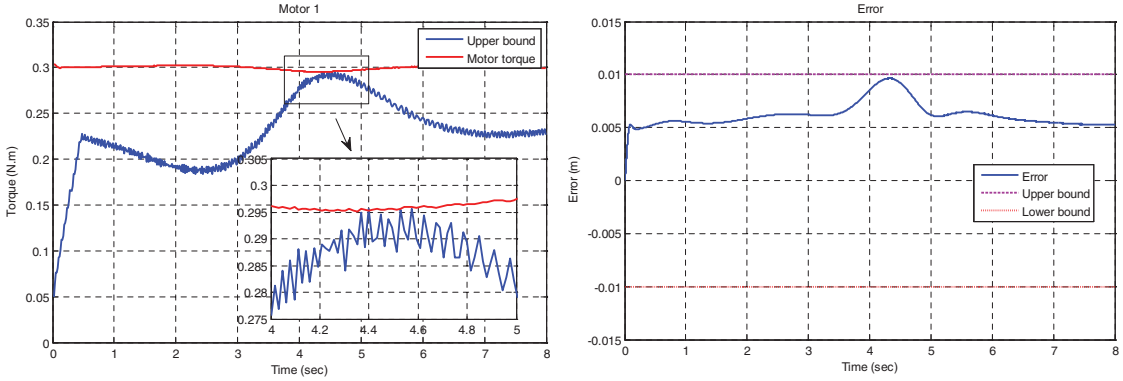
https://doi.org/10.1017/S0263574714000472 Published online by Cambridge University Press

Table VII. mDLCC and simulation parameters for flexible cable cases.

Name	Elasticity modulus (E)	Cable density (ρ)	Control gain (λ)	Control gain (K)	DLCC (kg)
Case 1	1.65×10^8 [N/m^2]	0.0125 [kg/m]	[2,6,40,14,0.4,4]	[10,8,160,22,8,4]	**3.85**
Case 2	1.65×10^7 [N/m^2]	0.0125 [kg/m]	[2,6,40,14,0.4,4]	[10,8,160,22,8,4]	**3.70**

Table VIII. DLCC of robot with two different controllers.

DLCC	Feedback linearization (kg)	Sliding mode (kg)
Rigid mode	4.65	4.65
Flexible joint	3.1	3.28
Flexible cable	3.2	3.7



(a) (b)

Fig. 14. Saturation profiles of flexible cable simulation for $E = 1.65 \times 10^8$ (a) torque constraint; (b) accuracy constraint.

3.7 kg, which is considerably lower than that of the rigid case one. It is clear that, by decreasing the elasticity modulus, the amplitude of cable vibration, and consequently, the amplitude of oscillation of the motors torque rise. This higher flexibility also reduces the robot accuracy. So it can be seen that the robot DLCC dwindles.

Furthermore, the DLCC of the robot with SMC controller is compared to the robot controlled by feedback linearization in three cases (Table VIII). This comparison is aimed on investigating the effects of a robust controller compared with non-robust one to reduce the effect of flexibility uncertainties. The results from,[23,24] and the results of, this paper are given in Table IX. As seen, there is no difference between the DLCC of both controllers for the rigid case. However, in the flexible joint robot, there is a bit of difference between the amounts of DLCCs. This diversity is the result of the ability of robust controller that can increase the robot accuracy and compensate for the flexibility uncertainty in the joints. In flexible cable, the improvement of dynamic of flexible cable and existence of SMC controller causes a great difference between the DLCCs.

3.5. Experimental verification

For a validation of the simulation results, the helicoidal tracking results are compared to those of the experimental test. Experimental tests are implemented on a 6-DOF under-constrained cable-suspended robot, ICaSbot, designed and manufactured in Iran University of Science and Technology (IUST).[25]

Six DC motors are responsible for supporting six suspended cables. The length change of these cables controls three translational and three rotational movements of a triangular shape end-effector. Three types of sensors including encoders, load cells, and the combination of camera and lasers are used to send the feedback signals of the robot movement. The ICaSbot main structure and different parts are shown in Fig. 15. Encoders measure the angular position and velocity of the motors. Load

https://doi.org/10.1017/S0263574714000472 Published online by Cambridge University Press

Table IX.The specifications of the robot and selected motor.[26].

Body			Motor
Height	120 cm	Type	DC gear motor
Side length of base triangle	100–120 cm	Model	Buehler 1.61.070
Weight	350 kg	Reference voltage	12 v
End-effector		No load speed	103 rpm
Side length of base	17 cm	Max torque	910 m N.m
Thickness	8 mm	Rated current	1.4 A
Weight	1100 g	Reduction ratio	1:25.2
		Weight	220 g

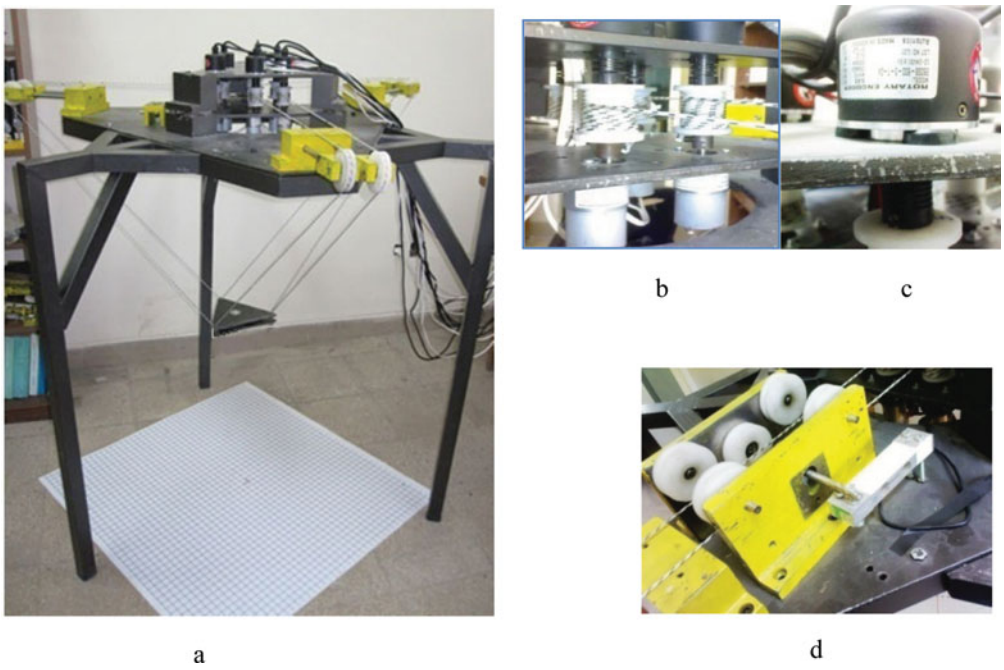


Fig. 15. (a) Scheme of the designed IUST cable robot;[26] (b) motors; (c) encoder; (d) load call.

cells measure the cable tension, and finally, the exact position of the end-effector is obtained by the combination of camera and lasers (Fig. 16). As it can be seen in Fig. 16, three laser sensors estimate the altitude and rotational movement of the end-effector, while camera records planer movement of the end-effector.[26]

In a previous work,[25] the robot was controlled in an open-loop scheme. Here, a robust closed-loop control scheme is installed on robot. Two sequential controlling loops are provided by which the motor is controlled in the inner loop, each 0.01 s, while the end-effector position is controlled in the outer loop, each 0.1 s. A closed-loop motor controller is designed as the inner loop. The motor speed is controlled using encoders' feedback. As shown in Fig. 17, the pulse-width modulation (PWM) commands (1 kHz frequency) are generated by controlling the signal and sending it directly to the motor.

The equations of helicoidal path are shown in Table X. The experimental tracking results are compared to flexible joint and flexible cable simulation.

A satisfactory degree of compatibility between the simulation and experimental results demonstrates the accuracy of simulation, necessity of flexibility modeling, and efficiency of implemented sliding mode controller.

As seen in Fig. 18(a), in x–y plane, modeling the joint flexibility provides a better evaluation of the real robot response rather than flexible cable case. By contrast, modeling the cable flexibility shows better compatibility with respect to the real robot response in z direction (Fig. 18(b)). It is attributed

https://doi.org/10.1017/S0263574714000472 Published online by Cambridge University Press

Table X. Helicoidal path equation.

$t < 4$	$t \geq 4$	$z = -(0.2/8)t + 1$
$x = 0.05\cos(4\pi t^2/64)$ $y = 0.05\sin(4\pi t^2/64)$	$x = 0.05\cos(4\pi(-t+8)^2/64)$ $y = -0.05\sin(4\pi(-t+8)^2/64)$	$\psi = 0$ $\Theta = 0$ $\varphi = 0$

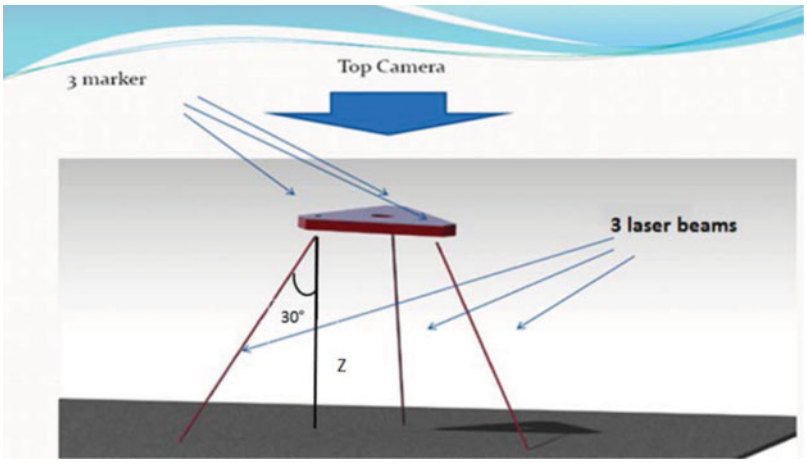


Fig. 16. The operation of camera and lasers to measure the end-effector position.[24]

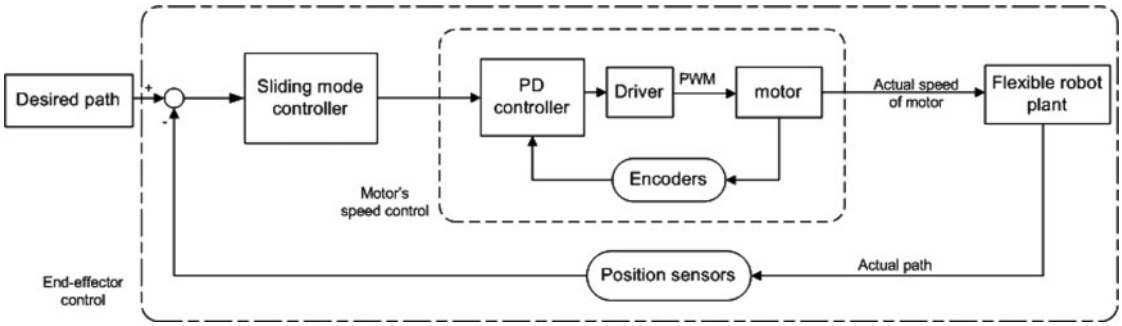


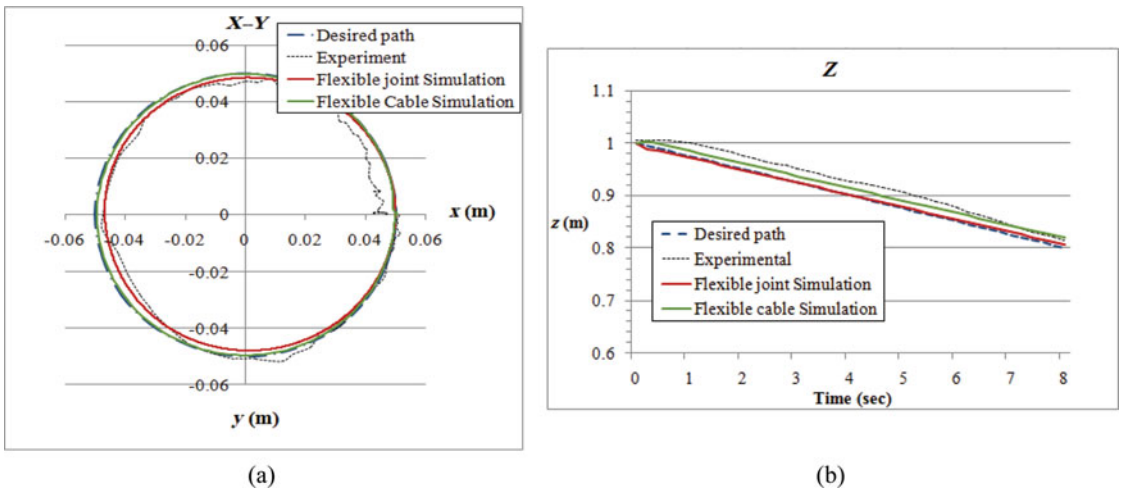
Fig. 17. Controlling strategy of flexible cable robot of ICaSbot.

to the fact that cable flexibility is modeled based on its longitudinal vibration, so the effect of height deviation is more evident here. However, in flexible joint case, this deviation is evident for all DOFs of the end-effector.

4. Conclusion

The present paper gives the design and implementation of a sliding mode controller to control a flexible cable-suspended robot which suffers from flexibility uncertainties. Two of the most significant uncertainties including joint flexibility and cable elasticity were modeled to reduce the probability of model uncertainty and provide a more complete dynamic model to evaluate the effect of flexibility on the robot. Flexibility of the cables with time-varying length was modeled for a cable-suspended robot with a novel approach. This approach is based on Newton's method and taking into account the cable large motions and its small longitudinal vibrating deformations simultaneously. The governing PDE of flexible cables dynamic was solved by the aid of Fourier transform. The SMC known as the robust method against uncertainties is implemented. Simulation of the trajectory tracking of the robot with flexible joint not only demonstrated the robustness of the designed sliding mode controller, but also it showed the impact of joint elasticity uncertainty on robot performance. An implication of these findings is that this uncertainty has greater impact on x–y plane of the end-effector tracking.

https://doi.org/10.1017/S0263574714000472 Published online by Cambridge University Press



(a) (b)

Fig. 18. Tracking of the end-effector in comparison to simulation results for a spiral path (a) *x*–*y* plane; (b) *z* direction.

Furthermore, by simulating the elastic cable robot with different modulus of elasticity, it was seen that there were continuous vibrations in trajectory tracking. Also, due to longitudinal vibration, there was always an offset along the *z* direction, while some oscillations are also observable around its mean value. Generally, it was concluded that modeling the flexibility for both the elastic joint and elastic cable leads to a considerable reduction in the DLCC of robot as the robot response has some deviation with respect to its rigid configuration. The validity of the results is verified by comparison of experimental results conducted on the ICaSbot robot. The simulation results demonstrate a good compatibility to experimental results. The above claim based on the main effect of cable flexibility on producing offset in *z* direction and the main effect of the joint flexibility in producing deviation in *x*–*y* plane was also approved by experimental comparisons.

References

1. J. Albus, R. Bostelman and N. Dagalakis, "The NIST robocrane," *J. Robot. Syst.* **10**(5), 709–724 (1993).
2. T. Brogårdh, "Present and future robot control development—an industrial perspective," *Annu. Rev. Control* **31**(1), 69–79 (2007).
3. N. Yanai, M. Yamamoto and A. Mohri, "Feedback Control for Wire-Suspended Mechanism with Exact Linearization," *Proceedings of the IEEE/RSJ International Conference on Intelligent Robots and Systems*, Lausanne, Switzerland, vol. 3, (Sept. 30–Oct. 4, 2002) pp. 2213–2218.
4. S. Oh and S. K. Agrawal, "A reference governor-based controller for a cable robot under input constraints," *IEEE Trans. Control Syst. Technol.* **13**(4), 639–645 (2005).
5. M. Zarebidoki, A. Lotfavar and H. R. Fahham, "Dynamic Modeling and Adaptive Control of a Cable-suspended Robot," *Proceedings of the World Congress on Engineering 2011*, vol. 3, London, UK (Jul. 6–8, 2011), *Lecture Notes in Engineering and Computer Science*, vol. 2192 (2011).
6. Y. Pi and X. Wang, "Observer-based cascade control of a 6-DOF parallel hydraulic manipulator in joint space coordinate," *Mechatronics* **20**(6), 648–655 (2010).
7. J. J. Gorman, K. W. Jablokow and D. J. Cannon, "The Cable Array Robot: Theory and Experiment," *Proceedings of the IEEE International Conference on Robotics and Automation*, Seoul, South Korea, vol. 3, (May 21–26, 2001) pp. 2804–2810.
8. S.-R. Oh, K. Mankala, S. K. Agrawal and J. S. Albus, "A dual-stage planar cable robot: Dynamic modeling and design of a robust controller with positive inputs," *J. Mech. Des.* **127**(4), 612–620 (2005).
9. S.-R. Oh, J.-C. Ryu and S. K. Agrawal, "Dynamics and control of a helicopter carrying a payload using a cable-suspended robot," *J. Mech. Des.* **128**(5), 1113–1121 (2006).
10. S.-R. Oh and S. K. Agrawal, "Nonlinear Sliding Mode Control and Feasible Workspace Analysis for a Cable Suspended Robot with Input Constraints and Disturbances," *Proceedings of the 2004 American Control Conference*, Boston, MA, USA, vol. 5, (Jun. 30–Jul. 2, 2004) pp. 4631–4636.
11. S.-R. Oh and S. K. Agrawal, "Guaranteed Reachable Domain and Control Design for a Cable Robot Subject to Input Constraints," *Proceedings of the 2005 American Control Conference*, Portland, OR, USA (Jun. 8–10, 2005) pp. 3379–3384.
12. J. S. Yeon and J. H. Park. "Practical Robust Control for Flexible Joint Robot Manipulators," *Proceedings of the IEEE International Conference on Robotics and Automation 2008*, Pasadena, CA, USA (May 19–23, 2008) pp. 3377–3382.

https://doi.org/10.1017/S0263574714000472 Published online by Cambridge University Press

13. M. H. Korayem, H. Tourajizadeh and M. Bamdad, "Dynamic load carrying capacity of flexible cable suspended robot: robust feedback linearization control approach," *J. Intell. Robot. Syst.* **60**(3–4), 341–363 (2010).
14. B. Zi, B. Y. Duan, J. L. Du and H. Bao, "Dynamic modeling and active control of a cable-suspended parallel robot," *Mechatronics* **18**(1), 1–12 (2008).
15. Y. Zhang, S. K. Agrawal and P. Hagedorn, "Longitudinal vibration modeling and control of a flexible transporter system with arbitrarily varying cable lengths," *J. Vib. Control* **11**(3), 431–456 (2005).
16. Y. Zhang, S. K. Agrawal and P. Hagedorn, "Modeling and control of flexible transporter system with arbitrarily time-varying cable lengths," In *ASME 2003 International Design Engineering Technical Conferences and Computers and Information in Engineering Conference*, Chicago, Illinois, USA, vol. 5 (September 2–6, 2003) pp. 389–398.
17. Y. Zhang, S. K. Agrawal and M. J. Piovoso, "Coupled Dynamics of Flexible Cables and Rigid End-Effector for a Cable Suspended Robot," *Proceedings of the American Control Conference 2006*, Minneapolis, MN, USA (Jun. 14–16, 2006) pp. 6.
18. H. Mounier and J. Rudolph, "Flatness-based control of nonlinear delay systems: A chemical reactor example," *Int. J. Control* **71**(5), 871–890 (1998).
19. J. Du, H. Bao C. Cui and D. Yang, "Dynamic analysis of cable-driven parallel manipulators with time-varying cable lengths," *Finite Elem. Anal. Des.* **48**(1), 1392–1399 (2012).
20. Q. J. Duan, J. L. Du, B. Y. Duan and A. F. Tang, "Deployment/retrieval modeling of cable-driven parallel robot," *Math. Probl. Eng.* 2010, 1–10 (2010).
21. A. B. Alp and S. K. Agrawal, Cable Suspended Robots: Design, Planning and Control *M.Sc Thesis* (Newark, NJ: Department of Mechanical Engineering, University of Delaware, 2001).
22. H. K. Khalil and J. W. Grizzle, *Nonlinear Systems*, vol. 3 (Prentice Hall, New Jersey, 2002).
23. M. H. Korayem and H. Tourajizadeh, "Maximum DLCC of spatial cable robot for a predefined trajectory within the workspace using closed loop optimal control approach," *J. Intell. Robot. Syst.* **63**(1), 75–99 (2011).
24. H. Tourajizadeh and M. H. Korayem, Control of Spatial Cable Robot Using Feedback Linearization Approach *M.S Thesis* (Tehran, Iran: Mechanical Department, Iran University of Science and Technology, 2008).
25. M. H. Korayem, M. Bamdad, H. Tourajizadeh, H. Shafiee, R. M. Zehtab and A. Iranpour, "Development of ICASBOT: A cable-suspended robot's with six DOF," *Arab. J. Sci. Eng.* **38**(5), 1–19 (2012).
26. M. H. Korayem, S. Khayatzadeh, H. Tourajizadeh and M. Taherifar, "Online recording the position and orientation of an end-effector of a spatial cable-suspended robot for close loop control using hybrid sensors," *J. Control Eng. Technol.* **3**(1), (2013).
27. R. N. Bracewell and R. N. Bracewell, *The Fourier Transform and its Applications*, vol. 31999 (McGraw-Hill, New York, 1986).

Appendix A

The Fourier transform to convert the PDE to ODE is carried out as:[27]

$$U_n = U_u\{u(s)\} = \int_0^L u(s)\cos\lambda_n s ds \tag{48}$$

$$\Rightarrow U_u\left\{u''(s)\right\} = -\lambda_n^2 U_n + \sqrt{\frac{2}{L}}\left[(-1)^{n+1}\lambda_n u(L) - u'(0)\right] \tag{49}$$

where:

$$\lambda_n = \frac{(2n-1)\pi}{2L} \tag{50}$$

The inverse Fourier transform can be obtained by the following equation:

$$u(s) = U_u^{-1}\{U(n)\} = \sqrt{\frac{1}{2L}}U_u(0) + \sqrt{\frac{2}{L}}\sum_{n=1}^{\infty} U_n \cos\lambda_n s \tag{51}$$

https://doi.org/10.1017/S0263574714000472 Published online by Cambridge University Press

Appendix B

Fourier cosine transform used to convert the PDE to ODE is[27]

$$U_c(n) = U_c\{u(s)\} = \frac{2}{L}\int_0^L u(s)\cos\lambda_n s ds \tag{52}$$

$$\Rightarrow U_c\left\{u''(s)\right\} = -\lambda_n^2 U_c(n) - \frac{2}{L}\left[u'(0) + (-1)^{n+1}u'(L)\right], \tag{53}$$

where

$$\lambda_n = \frac{n\pi}{L}. \tag{54}$$

The cosine inverse Fourier transform is

$$u(s) = U_c^{-1}\{U_c(n)\} = \frac{U_c(0)}{2} + \sum_{n=1}^{\infty} U_c(n)\cos\lambda_n s. \tag{55}$$

https://doi.org/10.1017/S0263574714000472 Published online by Cambridge University Press